TRANSACTIONS
OF TIANJIN UNIVERSITY

2016, 22: 358-366
DOI 10.1007/s12209-016-2838-0

Multiframe Blind Super Resolution Imaging Based on Blind Deconvolution*

Yuan Wei(元　伟)[1], Zhang Liyi(张立毅)[1,2]
(1. School of Electronic Information Engineering, Tianjin University, Tianjin 300072, China;
2. College of Information Engineering, Tianjin University of Commerce, Tianjin 300134, China)

Abstract: As an ill-posed problem, multiframe blind super resolution imaging recovers a high resolution image from a group of low resolution images with some degradations when the information of blur kernel is limited. Note that the quality of the recovered image is influenced more by the accuracy of blur estimation than an advanced regularization. We study the traditional model of the multiframe super resolution and modify it for blind deblurring. Based on the analysis, we proposed two algorithms. The first one is based on the total variation blind deconvolution algorithm and formulated as a functional for optimization with the regularization of blur. Based on the alternating minimization and the gradient descent algorithm, the high resolution image and the unknown blur kernel are estimated iteratively. By using the median shift and add operator, the second algorithm is more robust to the outlier influence. The MSAA initialization simplifies the interpolation process to reconstruct the blurred high resolution image for blind deblurring and improves the accuracy of blind super resolution imaging. The experimental results demonstrate the superiority and accuracy of our novel algorithms.

Keywords: blind deconvolution; multiframe blind super resolution imaging; regularization; iteration; deblurring

Blind super resolution imaging (BSRI) has been active recently in the field of digital image processing since the seminal research[1-3]. BSRI is a set of techniques which reconstruct one or some high resolution (HR) images from one or some low resolution (LR) images with the limited information of blur.

Recently, the traditional super resolution imaging (SRI) methods are usually functional under the assumption of a known blur, e.g., Gaussian blur kernel[4,5], averaging blur kernel[6], etc. However, in actual situation, there are many unknown, different and complicated blur kernels in the LR images. Compared with BSRI methods, the traditional SRI methods are prevented from recovering HR image accurately by the unknown blur[3]. And BSRI methods are more challenging and complicated than the traditional SRI methods. According to the seminal work in Ref. [7], the accuracy of blur estimation is more crucial to the accurate reconstruction of the HR image than a sophisticated image prior. So there is a significant positive correlation between the accuracy of blur estimation and that of HR image estimation.

In order to improve the quality of the HR image, some relevant works focusing on the blur estimation have shown the state-of-the-art performance. A parametric model with the assumption of Gaussian blur kernel was proposed in Ref. [8]. But the method cannot achieve a high-quality image if the actual blur is a comprehensive combination of motion blur, out-of-focus blur, etc. In Ref. [9] an incremental expectation maximization framework was adopted to deal with the SRI problem based on multiframe blind deconvolution successfully. Ref. [10] confirmed that if the image size is large enough, the MAP_k method would converge to the true solution. In Ref. [11] a modified total variation blind deconvolution (TVBD) method was presented to recover both blur kernels and images with higher speed and accuracy. By using the MAP_k model based on nonparametric prior to estimating blur kernels, the authors in Ref. [12] resorted

Accepted date: 2016-03-31.
*Supported by the National Natural Science Foundation of China (No. 61340034), the Research Program of Application Foundation and Advanced Technology of Tianjin (No.13JCYBJC15600).
Yuan Wei, born in 1980, male, doctorate student.
Correspondence to Yuan Wei, E-mail: reganyuan888@126.com.

to the inherent patch recurrence at different image scales to achieve a significant SRI improvement. They utilized both the methods in Ref. [13] and Ref. [14] to test their method for single blind super resolution imaging (SBSRI). Multiframe blind super resolution imaging (MBSRI) can fuse far more non-redundant information by using the subpixel interpolation from many similar LR images. So the image details recovered in Ref. [12] are not as good as those recovered by MBSRI.

Because of the difficulties, only few works focus on this topic. Outliers and cumulative errors from LR image sequence are not modeled explicitly and have a great influence on the final result. The authors in Ref. [13] proposed two robust methods to solve the multiframe SRI problem with a known Gaussian blur. And the second one is based on "median shift and add" (MSAA) operation[13] and can overcome the outlier influence with a higher speed. However, their methods cannot solve the BSRI problem.

As a classical inverse problem, image deconvolution is ill-posed on account of the ill-conditioned nature of the convolution operators[14]. Ref. [10] showed that the joint optimization of the unknowns can achieve the no-blur solution. Ref. [11] showed that if all the required constraints are imposed simultaneously, the algorithm may not converge to a no-blur solution independent of regularization. This is the reason why so many joint optimization algorithms have desirable convergence[15,16]. Nevertheless, there is some gap between blind deconvolution and BSRI, because BSRI is more complicated due to image interpolation, image registration, LR-HR patches query, etc, while blind deconvolution just solves the deblurring problem.

In the paper, we study the traditional observation models of super resolution and present our model of MBSRI. A combined algorithm based on total variation blind deconvolution (TVBD) is proposed. The algorithm can handle the comprehensive blur, which is combined with many different and complicated blur kernels. In order to remove the outliers from the LR images, we propose a combined MBSRI algorithm based on MSAA. The simulation results demonstrate the efficiency and accuracy of our algorithms.

1 Multiframe super resolution

The LR images result from the degradations (i.e., geometric transformation, blurring and downsampling) in the acquisition process. There are two traditional observation models for multiframe super resolution imaging (MSRI).

The first model only considers the point spread function (PSF) of imaging hardware such as digital cameras, digital scanners and digital video-equipment[13,17,18], and it is shown as follows

$$\boldsymbol{Y}_c = \boldsymbol{D}_c \boldsymbol{H}_c^{\mathrm{sys}} \boldsymbol{F}_c \boldsymbol{X} + \boldsymbol{V}_c \qquad c = 1, \cdots, N \tag{1}$$

where $\boldsymbol{Y}_c$ encodes the cth LR image from the imaging system and it is arranged as an $m^2 \times 1$ vector; $m^2 \times r^2 m^2$ matrix $\boldsymbol{D}_c$ is the cth downsampling operator; $r^2 m^2 \times r^2 m^2$ matrix $\boldsymbol{H}_c^{\mathrm{sys}}$ is the cth blur kernel of imaging system, and is usually assumed to be the same as the other blur kernels if using only one digital camera, and r is the super resolution enhancement factor; $r^2 m^2 \times r^2 m^2$ matrix $\boldsymbol{F}_c$ models the cth geometric transformation or motion; $r^2 m^2 \times 1$ vector $\boldsymbol{X}$ is the desired HR image, and $m^2 \times 1$ vector $\boldsymbol{V}_c$ is the cth noise term. All the LR and HR images are arranged in a lexicographical order.

The second observation model only considers the blur effects from the outside, such as the linear motion blur. Let $r^2 m^2 \times r^2 m^2$ matrix $\boldsymbol{H}_c$ denote the cth blur kernel, and the model is defined as

$$\boldsymbol{Y}_c = \boldsymbol{D}_c \boldsymbol{F}_c \boldsymbol{H}_c \boldsymbol{X} + \boldsymbol{V}_c \qquad c = 1, \cdots, N \tag{2}$$

According to Ref. [13], the two models are combined together and a general observation model is obtained as

$$\boldsymbol{Y}_c = \boldsymbol{D}_c \boldsymbol{H}_c^{\mathrm{sys}} \boldsymbol{F}_c \boldsymbol{H}_c \boldsymbol{X} + \boldsymbol{V}_c = \boldsymbol{D}_c \boldsymbol{H}_c^{\mathrm{sys}} \boldsymbol{H}_c \boldsymbol{F}_c \boldsymbol{X} + \boldsymbol{V}_c \qquad c = 1, \cdots, N \tag{3}$$

The general model under their assumption (i.e., $\boldsymbol{F}_c$, $\boldsymbol{H}_c^{\mathrm{sys}}$ and $\boldsymbol{H}_c$ are block circulant matrices) only focuses on the known blur kernels and they merge the two kernels as one. We just give a brief review here and more details can be found in Ref. [13].

The general model is shown in Fig. 1.

Fig. 1 General observation model for MSRI

However, when the information of the blur is limited, their model is more complicated to handle the blind deconvolution. So we change their model into a novel one under the same assumption[13] for simplified computation and define it for image deblurring as

$$\boldsymbol{Y}_c = \boldsymbol{D}_c\boldsymbol{F}_c\boldsymbol{H}_c^{\mathrm{sys}}\boldsymbol{H}_c\boldsymbol{X} + \boldsymbol{V}_c = \boldsymbol{D}_c\boldsymbol{F}_c\boldsymbol{H}_{\mathrm{com}}\boldsymbol{X} + \boldsymbol{V}_c \qquad c = 1,\cdots,N \tag{4}$$

where $r^2m^2 \times r^2m^2$ matrix $\boldsymbol{H}_{\mathrm{com}}=\boldsymbol{H}_c^{\mathrm{sys}}\boldsymbol{H}_c$. We can treat $\boldsymbol{H}_{\mathrm{com}}\boldsymbol{X}$ as a blurry HR image in the MBSRI process, as shown in Fig. 2.

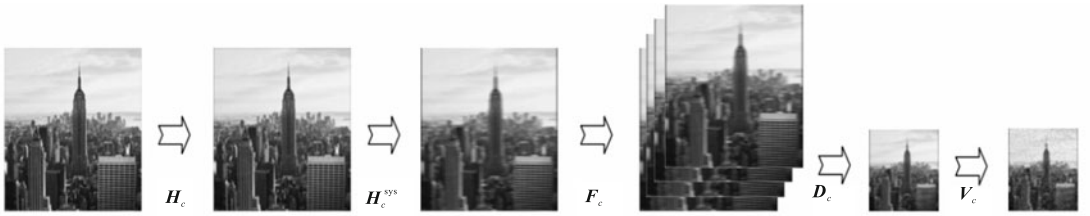

Fig. 2 Modified general observation model for MBSRI

2 Multiframe blind super resolution imaging

2.1 Blind deconvolution based on total variation

Total variation (TV) is one of the most popular priors for recovering image and blur kernel[11, 19]. Ref. [10] showed that $\mathrm{MAP_k}$ can yield the desired solution when using a uniform distribution for the unknown blur and a TV prior for the image gradients. The authors in Ref. [20] argued that the conclusions are right, while by using the sparse-inducing prior, the classical $\mathrm{MAP_{u,k}}$ algorithm cannot yield the no-blur solution. A modified method based on TVBD was introduced in Ref. [11], as follows

$$\min_{\boldsymbol{u},\boldsymbol{k}} \ \|\boldsymbol{k}*\boldsymbol{u}-\boldsymbol{f}\|_2^2 + \lambda \mathrm{TV}(\boldsymbol{u})$$
$$\text{s.t.} \qquad k_{i,j} \geqslant 0, \quad \|\boldsymbol{k}\|_1 = 1 \tag{5}$$

where $\boldsymbol{k}$, $\boldsymbol{u}$ and $\boldsymbol{f}$ are blur kernel, sharp image and blurred image, respectively. TV is the regularization for $\boldsymbol{u}$. Alternating minimization (AM) is used to change the nonconvex cost function into two cost functions. One function estimates $\boldsymbol{u}$ and it is defined as

$$\boldsymbol{u}^t \leftarrow \arg\min_{\boldsymbol{u}} \|\boldsymbol{k}^{t-1}*\boldsymbol{u}-\boldsymbol{f}\|_2^2 + \lambda \mathrm{TV}(\boldsymbol{u}) \tag{6}$$

The other one estimates $\boldsymbol{k}$ and it is defined as

$$\boldsymbol{k}^t \leftarrow \arg\min_{\boldsymbol{k}} \|\boldsymbol{k}*\boldsymbol{u}^t-\boldsymbol{f}\|_2^2$$
$$\text{s.t.} \qquad k_{i,j} \geqslant 0, \quad \|\boldsymbol{k}\|_1 = 1 \tag{7}$$

By using the gradient descent algorithm to calculate both of them, the constraints on the unknown blur are used to avoid the no-blur solution. The iteration on $\boldsymbol{u}$ is

$$\boldsymbol{u}^t \leftarrow \boldsymbol{u}^{t-1} - \mu_u\left(\boldsymbol{k}_-^{t-1} * (\boldsymbol{k}^{t-1} \odot \boldsymbol{u}^{t-1} - \boldsymbol{f}) - \lambda\nabla\cdot\frac{\nabla\boldsymbol{u}^{t-1}}{|\nabla\boldsymbol{u}^{t-1}|}\right) \tag{8}$$

where the notation * is the discrete convolution operator that can obtain the full 2-dimensional convolution result; $\odot$ indicates the discrete convolution on the valid part without the zero-padded edges; ∇ is the Nabla symbol and denotes the gradient; and $\boldsymbol{k}\_(a) = \boldsymbol{k}(-a)$.

The iteration on $\boldsymbol{k}$ is

$$\boldsymbol{k}^{t-1} \leftarrow \boldsymbol{k}^{t-1} - \mu_k(\boldsymbol{u}_-^t \odot (\boldsymbol{k}^{t-1} \odot \boldsymbol{u}^t - \boldsymbol{f})) \tag{9}$$

The $\boldsymbol{k}$ constraints resort to the sequential projection and they are given by

$$\boldsymbol{k}^{(t-1)+1/3} \leftarrow \boldsymbol{k}^{t-1} \tag{10}$$

$$\boldsymbol{k}^{(t-1)+2/3} \leftarrow \max\{\boldsymbol{k}^{(t-1)+1/3}, 0\} \tag{11}$$

$$\boldsymbol{k}^t \leftarrow \frac{\boldsymbol{k}^{(t-1)+2/3}}{\|\boldsymbol{k}^{(t-1)+2/3}\|_1} \tag{12}$$

In order to improve the speed and accuracy of the algorithm, the TVBD method is modified by using pyramid scheme and free-boundary implementation[11]. The method[11] is shown as follows.

Algorithm: TVBD

Input data: $\boldsymbol{f}$, size of $\boldsymbol{k}$, initial $\boldsymbol{u}$, λ , $\lambda_{\min}$

Output results: $\boldsymbol{u}$, $\boldsymbol{k}$

(1) $\boldsymbol{u}^0 \leftarrow \mathrm{pad}(\boldsymbol{f})$

(2) $\boldsymbol{k}^0 \leftarrow$ uniform

(3) while not converged do

(4) $\boldsymbol{u}^{t+1} \leftarrow \boldsymbol{u}^t - \mu_u\left(\boldsymbol{k}_-^t * (\boldsymbol{k}^t \odot \boldsymbol{u}^t - \boldsymbol{f}) - \lambda\nabla\cdot\frac{\nabla\boldsymbol{u}^t}{|\nabla\boldsymbol{u}^t|}\right)$

(5) $\boldsymbol{k}^{t+1/3} \leftarrow \boldsymbol{k}^t - \mu_k(\boldsymbol{u}_-^{t+1} \odot (\boldsymbol{k}^t \odot \boldsymbol{u}^{t+1} - \boldsymbol{f}))$

(6) $\boldsymbol{k}^{t+2/3} \leftarrow \max\{\boldsymbol{k}^{t+1/3}, 0\}$

(7) $\boldsymbol{k}^{t+1} \leftarrow \frac{\boldsymbol{k}^{t+2/3}}{\|\boldsymbol{k}^{t+2/3}\|_1}$

(8) $\lambda \leftarrow \max\{0.999\lambda, \lambda_{\min}\}$

(9) $t \leftarrow t+1$

(10) end

(11) $\boldsymbol{u} \leftarrow \boldsymbol{u}^{t+1}$

(12) $\boldsymbol{k} \leftarrow \boldsymbol{k}^{t+1}$

2.2 Multiframe blind super resolution imaging based on TVBD

In Section 1, we study the modified general observation model for MBSRI. Based on the above model, by using the least-squares-based super resolution, we can resort to the L_1 norm estimator to obtain a robust blurred HR image. In Ref. [13], it has been proved to be the most robust cost function for it gets the highest breakpoint value.

Because blind super resolution is an ill-posed inverse problem, the effective regularization term should be used to get a stable solution with higher accuracy and more details. To remove the outliers and the other measurement errors, the regularization process usually removes the sharp edges with similar high-frequency energy. On the contrary, when handling the blind deconvolution, the regularization term may cause some unwanted artifacts with some high frequency energy, which means that the choice of the regularization term is far more important for the final results.

We find that TV and bilateral TV (BTV) are proper regularization terms. Both of them can be used to reduce the visible noise effectively. TV penalizes the total amount of the image differences in horizontal (x) and vertical (y) directions.

L_1-norm-based TV is given by

$$\mathrm{TV}(\boldsymbol{X}) = \sum_i \left|\nabla_i^x \boldsymbol{X}\right| + \left|\nabla_i^y \boldsymbol{X}\right| \tag{13}$$

L_2-norm-based TV is given by

$$\mathrm{TV}(\boldsymbol{X}) = \sum_i \sqrt{\left(\nabla_i^x \boldsymbol{X}\right)^2 + \left(\nabla_i^y \boldsymbol{X}\right)^2} \tag{14}$$

BTV is defined as

$$\mathrm{BTV}(\boldsymbol{X}) = \underbrace{\sum_{l=-P}^{P}\sum_{m=0}^{P}}_{l+m\geqslant 0} \alpha^{|l|+|m|} \left\|\boldsymbol{X} - \boldsymbol{S}_x^l \boldsymbol{S}_y^m \boldsymbol{X}\right\|_1 \tag{15}$$

where the matrices $\boldsymbol{S}_x^l$ and $\boldsymbol{S}_y^m$ shift the image $\boldsymbol{X}$ by l and m units (pixels) in x and y directions; their transposes are $\boldsymbol{S}_x^{-l}$ and $\boldsymbol{S}_y^{-m}$, which shift $\boldsymbol{X}$ in the opposite directions correspondingly; α is a positive scalar weight, i.e., $\alpha \in (0,1)$, and the summation of image variation is spatially influenced by it. More details can be found in Ref. [13].

When the noisy image contains some details and edges, BTV is more robust and accurate to recover the image and preserve the high-frequency information than TV, because BTV considers more pixels in a larger neighboring region. However, we find that BTV is not as good as TV in the process of blind deconvolution and causes more artifacts in the reconstructed images, while TV can achieve a better result of the blind image deblurring.

The goal of blind super resolution imaging is to improve the image details as much as possible, so that the recovered image turns out to be far closer to the ground-truth image. We study both the advantages and disadvantages of TV and BTV, and combine them together to propose an MBSRI algorithm based on TVBD in Ref. [11]. Our algorithm resorts to L_1-norm-based fidelity term and BTV regularization term to reconstruct a blurry HR image from a set of LR images; and then the TVBD algorithm is utilized to recover the blur kernel and the HR image simultaneously in the way of alternating minimization. The algorithm based on maximum *a posteriori* (MAP) is formulated as

$$\begin{cases} \boldsymbol{Z} = \arg\min\limits_{\boldsymbol{Z}} \sum\limits_{c=1}^{N} \left\|\boldsymbol{D}\boldsymbol{F}_c\boldsymbol{Z} - \boldsymbol{Y}_c\right\|_1 + \lambda' \mathrm{BTV}(\boldsymbol{Z}) \\ \boldsymbol{u}, \boldsymbol{k} = \arg\min\limits_{\boldsymbol{u},\boldsymbol{k}} \left\|\boldsymbol{k} * \boldsymbol{u} - \boldsymbol{Z}\right\|_2^2 + \\ \qquad\qquad \lambda \mathrm{TV}(\boldsymbol{u}) + \gamma \mathrm{TV}(\boldsymbol{k}) \\ \text{s.t.} \quad \left\|\boldsymbol{k}\right\|_1 = 1, \quad k_{i,j} \geqslant 0 \end{cases} \tag{16}$$

where $\boldsymbol{D}$ is downsampling operator; $\boldsymbol{Z}$ is blurry HR image. The gradient descent method is used for the minimization of cost functions. In the algorithm model, we add a regularization term for the blur kernel to keep its sharp details. λ and γ can be achieved by predicted SURE method[21], projected SURE method[22] and nonlinear generalized cross-validation (NGCV) method[23], and can be set adaptively iteration by iteration to get accurate results in the same way as Perrone's TVBD method[11]. More details can be found in Ref. [11]. If we set the blur weight γ to zero, the model would be the original TVBD algorithm in Ref. [11], and the model seems more general. λ' can be selected by using the methods mentioned above.

The pseudo-code of the proposed algorithm is expressed as follows.

Algorithm: MBSRI algorithm based on TVBD

Input data: $\boldsymbol{D}_c$, $\boldsymbol{Y}_c$, size of $\boldsymbol{k}$, λ', λ, γ, $\lambda_{\min}$, $\gamma_{\min}$

Output results: $\boldsymbol{u}$, $\boldsymbol{k}$

(1) image registration based on the optical flow method to estimate $\boldsymbol{F}_c$

(2) $\boldsymbol{k}^0 \leftarrow$ uniform

(3) initialize the blurred HR image $\boldsymbol{Z}_0$ by using spline method

(4) while not converged do

(5) $\boldsymbol{Z}_{n+1} \leftarrow \boldsymbol{Z}_n - \beta[\sum_{c=1}^{N} \boldsymbol{F}_c^{\mathrm{T}} \boldsymbol{D}_c^{\mathrm{T}} \mathrm{sign}(\boldsymbol{D}_c \boldsymbol{F}_c \boldsymbol{Z}_n - \boldsymbol{Y}_c) + \lambda' \underbrace{\sum_{l=-P}^{P} \sum_{m=0}^{P}}_{l+m\geqslant 0} \alpha^{|l|+|m|} (\boldsymbol{I} - \boldsymbol{S}_y^{-m} \boldsymbol{S}_x^{-l}) \mathrm{sign}(\boldsymbol{Z}_n - \boldsymbol{S}_x^{l} \boldsymbol{S}_y^{m} \boldsymbol{Z}_n)]$

(6) $n \leftarrow n+1$

(7) end

(8) $\boldsymbol{u}^0 \leftarrow \mathrm{pad}(\boldsymbol{Z})$

(9) while not converged do

(10) $\boldsymbol{u}^{t+1} \leftarrow \boldsymbol{u}^t - \mu_u (\boldsymbol{k}_-^t * (\boldsymbol{k}^t \odot \boldsymbol{u}^t - \boldsymbol{Z}) - \lambda \nabla \cdot \frac{\nabla \boldsymbol{u}^t}{|\nabla \boldsymbol{u}^t|})$

(11) $\boldsymbol{k}^{t+1/3} \leftarrow \boldsymbol{k}^t - \mu_k (\boldsymbol{u}_-^{t+1} \odot (\boldsymbol{k}^t \odot \boldsymbol{u}^{t+1} - \boldsymbol{Z}) - \gamma \nabla \cdot \frac{\nabla \boldsymbol{k}^t}{|\nabla \boldsymbol{k}^t|})$

(12) $\boldsymbol{k}^{t+2/3} \leftarrow \max\{\boldsymbol{k}^{t+1/3}, 0\}$

(13) $\boldsymbol{k}^{t+1} \leftarrow \frac{\boldsymbol{k}^{t+2/3}}{\|\boldsymbol{k}^{t+2/3}\|_1}$

(14) $\lambda \leftarrow \max\{0.999\lambda, \lambda_{\min}\}$

(15) $\gamma \leftarrow \max\{0.999\gamma, \gamma_{\min}\}$

(16) $t \leftarrow t+1$

(17) $\mu_u = 5\times 10^{-3} \max(u_{i,j}) / \max(|\mathrm{grad} u_{i,j}|)$

(18) $\mu_k = 1\times 10^{-3} \max(k_{i,j}) / \max(|\mathrm{grad} k_{i,j}|)$

(19) end

(20) $\boldsymbol{k} \leftarrow \boldsymbol{k}^{t+1}$

(21) $\boldsymbol{u} \leftarrow \boldsymbol{u}^{t+1}$

(22) crop $\boldsymbol{u}$ according to Step (8) as the final result

Note that $\boldsymbol{D}_c^{\mathrm{T}}$ and $\boldsymbol{F}_c^{\mathrm{T}}$ are the transposes of $\boldsymbol{D}_c$ and $\boldsymbol{F}_c$ respectively; β is the step size of $\boldsymbol{Z}$; μ_k and μ_u are the step sizes of $\boldsymbol{k}$, $\boldsymbol{u}$ and they are self-adaptive to improve the performance of blind deblurring. In many papers such as Ref. [13], $\boldsymbol{D}_c$ is assumed to be the same (i.e., $\boldsymbol{D}_c$ is $\boldsymbol{D}$) and known.

2.3 Multiframe blind super resolution imaging based on median shift and add

In order to remove the outliers, all the LR images are classified according to the geometric transformation, i.e., the LR images with the same geometric transformation are in the same group. MSAA is applied to LR images in each group to obtain a median LR image. By using geometric transformation, a median HR image is interpolated by all the median LR images in a non-iterative process. The median HR image is used as an initial observation of the blurred HR image for blind image deblurring. For under-determined cases[13], some undefined pixels may cause the "hole" effect. To solve this problem, we adopt a spline method to upsample the first median LR image as a reference frame and then fuse the other median LR images together. Note that a better upsampling method can improve the final result.

With the assumption of known blur, the authors in Ref. [13] presented a fast method. They used some square Gaussian kernels to blur the images for simulation. Our algorithm based on MSAA combines their model with TVBD algorithm to solve the MBSRI problem in the case of outliers.

Our algorithm is formulated as

$$\begin{cases} \boldsymbol{Z} = \arg\min\limits_{\boldsymbol{Z}} \ \|\boldsymbol{A}\boldsymbol{Z} - \boldsymbol{A}\hat{\boldsymbol{Z}}\|_1 + \lambda' \mathrm{BTV}(\boldsymbol{Z}) \\ \boldsymbol{u}, \boldsymbol{k} = \arg\min\limits_{\boldsymbol{u},\boldsymbol{k}} \ \|\boldsymbol{k} * \boldsymbol{u} - \boldsymbol{Z}\|_2^2 + \lambda \mathrm{TV}(\boldsymbol{u}) \\ \text{s.t.} \quad \|\boldsymbol{k}\|_1 = 1, \quad k_{i,j} \geqslant 0 \end{cases} \tag{17}$$

where $\hat{\boldsymbol{Z}}$ is the median HR image; and $\boldsymbol{A}$ is a diagonal matrix. Every diagonal value is the positive square root of the number of LR images in the same group and more details about $\boldsymbol{A}$ can be found in Ref. [13]. By using MSAA, downsampling operator, geometric transformation and summation are removed from the iteration. This simplifies and accelerates the implementation. The outliers can be removed effectively when there are enough LR images. For example, the number of LR images should be $3r^2$ at least in the square cases. The proposed algorithm is expressed as follows.

Algorithm: MBSRI algorithm based on MSAA

Input data: $\boldsymbol{D}_c$, $\boldsymbol{Y}_c$, size of $\boldsymbol{k}$, λ', λ, $\lambda_{\min}$

Output results: $\boldsymbol{u}$, $\boldsymbol{k}$

(1) image registration based on the optical flow method to estimate $\boldsymbol{F}_c$

(2) $\boldsymbol{k}^0 \leftarrow$ uniform

(3) initialize the blurred HR image $\boldsymbol{Z}_0$ by using spline method and the median HR image by using MSAA

(4) while not converged do

(5) $\boldsymbol{Z}_{n+1} \leftarrow \boldsymbol{Z}_n - \beta[\boldsymbol{A}^{\mathrm{T}} \mathrm{sign}(\boldsymbol{A}\boldsymbol{Z}_n - \boldsymbol{A}\hat{\boldsymbol{Z}}) + \lambda' \underbrace{\sum_{l=-P}^{P} \sum_{m=0}^{P}}_{l+m\geqslant 0} \alpha^{|l|+|m|} (\boldsymbol{I} - \boldsymbol{S}_y^{-m} \boldsymbol{S}_x^{-l}) \mathrm{sign}(\boldsymbol{Z}_n - \boldsymbol{S}_x^{l} \boldsymbol{S}_y^{m} \boldsymbol{Z}_n)]$

(6) $n \leftarrow n+1$

(7) end

(8) $\boldsymbol{u}^0 \leftarrow \mathrm{pad}(\boldsymbol{Z})$

(9) while not converged do

(10) $\boldsymbol{u}^{t+1} \leftarrow \boldsymbol{u}^t - \mu_u (\boldsymbol{k}_-^t * (\boldsymbol{k}^t \odot \boldsymbol{u}^t - \boldsymbol{Z}) - \lambda \nabla \cdot \frac{\nabla \boldsymbol{u}^t}{|\nabla \boldsymbol{u}^t|})$

(11) $\boldsymbol{k}^{t+1/3} \leftarrow \boldsymbol{k}^t - \mu_k (\boldsymbol{u}_-^{t+1} \odot (\boldsymbol{k}^t \odot \boldsymbol{u}^{t+1} - \boldsymbol{Z}))$

(12) $\boldsymbol{k}^{t+2/3} \leftarrow \max\{\boldsymbol{k}^{t+1/3}, 0\}$

(13) $\boldsymbol{k}^{t+1} \leftarrow \dfrac{\boldsymbol{k}^{t+2/3}}{\left\|\boldsymbol{k}^{t+2/3}\right\|_1}$

(14) $\lambda \leftarrow \max\{0.999\lambda, \lambda_{\min}\}$

(15) $t \leftarrow t+1$

(16) $\mu_u = 5\times10^{-3}\max(u_{i,j})/\max(|\text{grad}u_{i,j}|)$

(17) $\mu_k = 1\times10^{-3}\max(k_{i,j})/\max(|\text{grad}k_{i,j}|)$

(18) end

(19) $\boldsymbol{k} \leftarrow \boldsymbol{k}^{t+1}$

(20) $\boldsymbol{u} \leftarrow \boldsymbol{u}^{t+1}$

(21) crop $\boldsymbol{u}$ according to Step (8) as the final result

Note that $\boldsymbol{A}^{\mathrm{T}}$ is the transpose matrix of $\boldsymbol{A}$ and they are equal.

3 Experiments

We have made some comparisons between the current state-of-the-art algorithms and our algorithm in this section. The online multiframe blind deconvolution (OMBD) algorithm[24] based on image deblurring method[25] achieves better results, and the blur kernel estimation (BKE) algorithm[26] shows the remarkable performance of blind deblurring. They are chosen for our comparisons and the no-blind robust super resolution method in Ref. [13] is adopted for BKE algorithm and TVBD algorithm. We use the dataset in Ref. [10] and create the data of LR images. Two experimental groups are used for the demonstration: in the first one, the proposed algorithms process 8 LR images of 123×123 pixels to estimate both kernel and HR image of 245×245 pixels in each experiment; in the second one, MBSRI algorithm based on MSAA processes 8 LR images of the same size with some heavy outliers to show its robust capability. All the simulations are implemented with MATLAB 2014a for Windows 7 X64 based on AMD Athlon 740 Quad Core CPU. In the experiments, the basic parameters are set as follows: $r=2$; $\alpha=0.01$; $\lambda_{\min}=6\times10^{-4}$; $\lambda'=0.001$; $\gamma_{\min}=2.4\times10^{-3}$; $P=2$; $\beta=3.95\times10^{-6}$.

The first group is performed to validate the accuracy of MBSRI based on TVBD and MBSRI based on MSAA. We evaluate the SSD and PSNR for the tests. In Figs. 3, 4 and 5, we show the recovered HR images and blur kernels achieved by OMBD, BKE, TVBD, and two new algorithms. From the figures, we can see that OMBD cannot estimate the blur kernel effectively with less LR images, and the original setting of saturation correction makes the HR images darker than the others, i.e., the image pixel values are quite lower than those of the ground truth images. As the blur kernels are more complicated and full of details, BKE cannot recover them effectively so that the recovered HR image is full of artifacts with a low degree of quality. Obviously influenced by the type of LR image or blur, BKE is not robust. Perrone's TVBD method[11] only focuses on the regularization for image, and shows a good performance. Visually, MBSRI based on TVBD is on a par with TVBD and improves the accuracy because of the regularization for blur. MBSRI based on MSAA outperforms the other algorithms in terms of quality and accuracy. Tabs. 1, 2 and 3 present the SSIM, PSNR (in dB), SSD and MSE separately corresponding to the experiments shown in Figs. 3, 4 and 5. According to these data, the proposed algorithms are superior to the others.

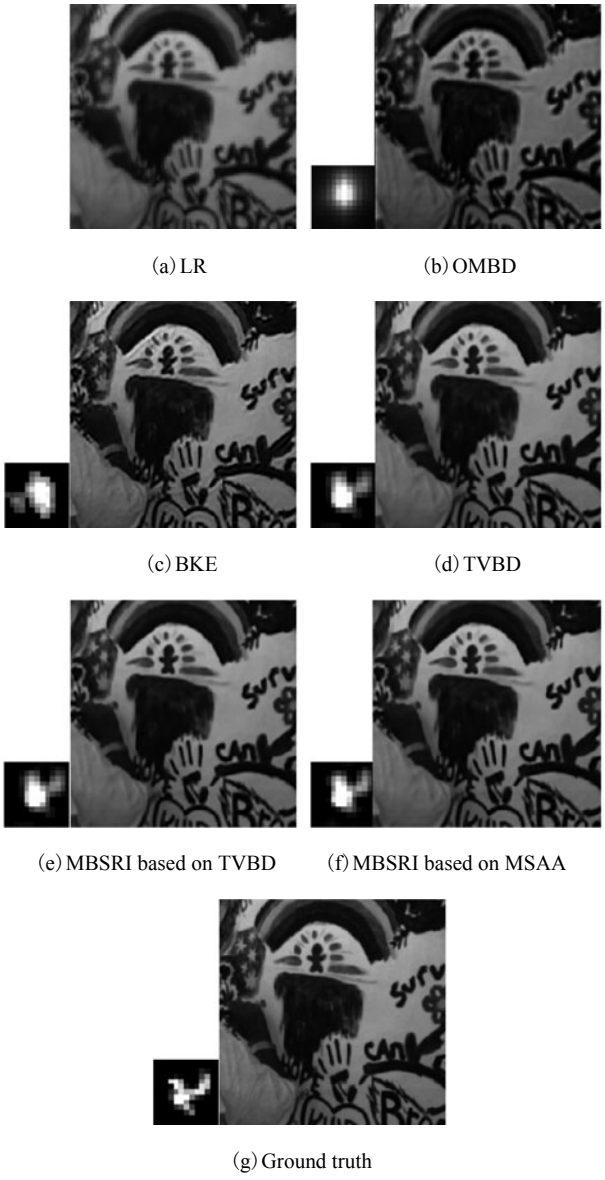

(a) LR (b) OMBD

(c) BKE (d) TVBD

(e) MBSRI based on TVBD (f) MBSRI based on MSAA

(g) Ground truth

Fig. 3 Results with the blur size of 13×13

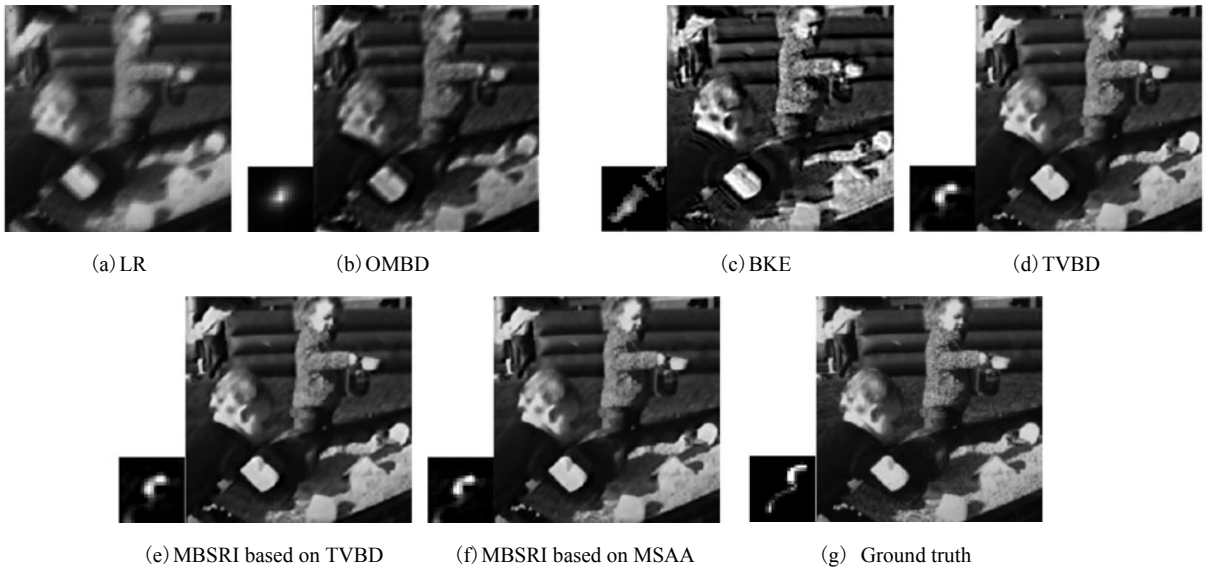

(a) LR (b) OMBD (c) BKE (d) TVBD

(e) MBSRI based on TVBD (f) MBSRI based on MSAA (g) Ground truth

Fig. 4 Results with the blur size of 21 × 21

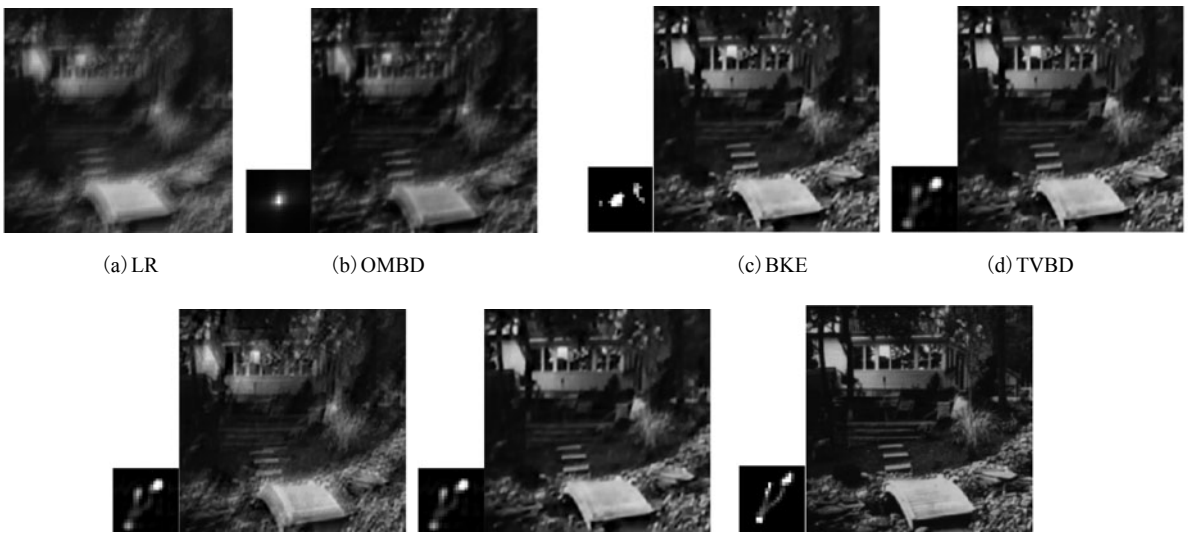

(a) LR (b) OMBD (c) BKE (d) TVBD

(e) MBSRI based on TVBD (f) MBSRI based on MSAA (g) Ground truth

Fig. 5 Results with the blur size of 23 × 23

Tab. 1 Comparison data of the experiment with the 13 × 13 blur kernel

Algorithm	SSIM	PSNR	SSD	MSE
BKE	0.936	30.283	43.308	9.369×10^{-4}
TVBD	0.971	34.279	17.256	3.733×10^{-4}
MBSRI based on TVBD	0.971	34.323	17.083	3.696×10^{-4}
MBSRI based on MSAA	0.975	35.013	14.574	3.153×10^{-4}

Tab. 2 Comparison data of the experiment with the 21 × 21 blur kernel

Algorithm	SSIM	PSNR	SSD	MSE
BKE	0.718	21.918	297.190	6.429×10^{-3}
TVBD	0.926	31.096	35.912	7.769×10^{-4}
MBSRI based on TVBD	0.926	31.122	35.702	7.724×10^{-4}
MBSRI based on MSAA	0.935	31.886	29.946	6.478×10^{-4}

Tab. 3 Comparison data of the experiment with the 23 × 23 blur kernel

Algorithm	SSIM	PSNR	SSD	MSE
BKE	0.671	21.375	336.817	7.287×10^{-3}
TVBD	0.869	28.306	68.286	1.477×10^{-3}
MBSRI based on TVBD	0.869	28.324	68.001	1.471×10^{-3}
MBSRI based on MSAA	0.887	29.162	56.066	1.213×10^{-3}

In the second experimental group, significant outlier effect is imposed to the LR images in order to test the robustness. In Fig. 6 and Fig. 7, we provide the comparison between our algorithm based on MSAA and OMBD, BKE, TVBD, TVBDL2. TVBDL2 is based on TVBD and the traditional super resolution method with a L_2 norm fidelity mentioned in Ref. [13]. From the simula-

tion, the outliers shown in Fig. 6(b) and Fig. 7(b) can obviously influence the results of TVBDL2 and OMBD respectively; BKE yields the HR images with some artifacts and TVBD seems robust; our algorithm can reconstruct both the HR image and the blur kernel more robustly and accurately than the others. Corresponding to the experimental results shown in Figs. 6 and 7, the data in Tabs. 4 and 5 demonstrate the superiority of our algorithm.

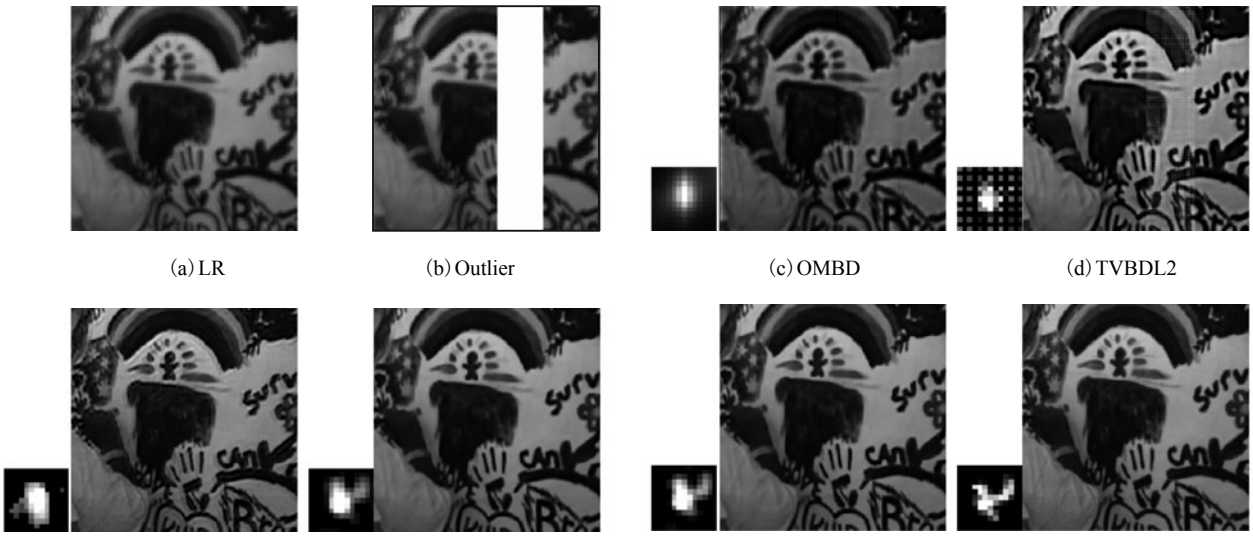

(a) LR (b) Outlier (c) OMBD (d) TVBDL2

(e) BKE (f) TVBD (g) MBSRI based on MSAA (h) Ground truth

Fig. 6 Results with the blur size of 13 × 13 and the outlier influence

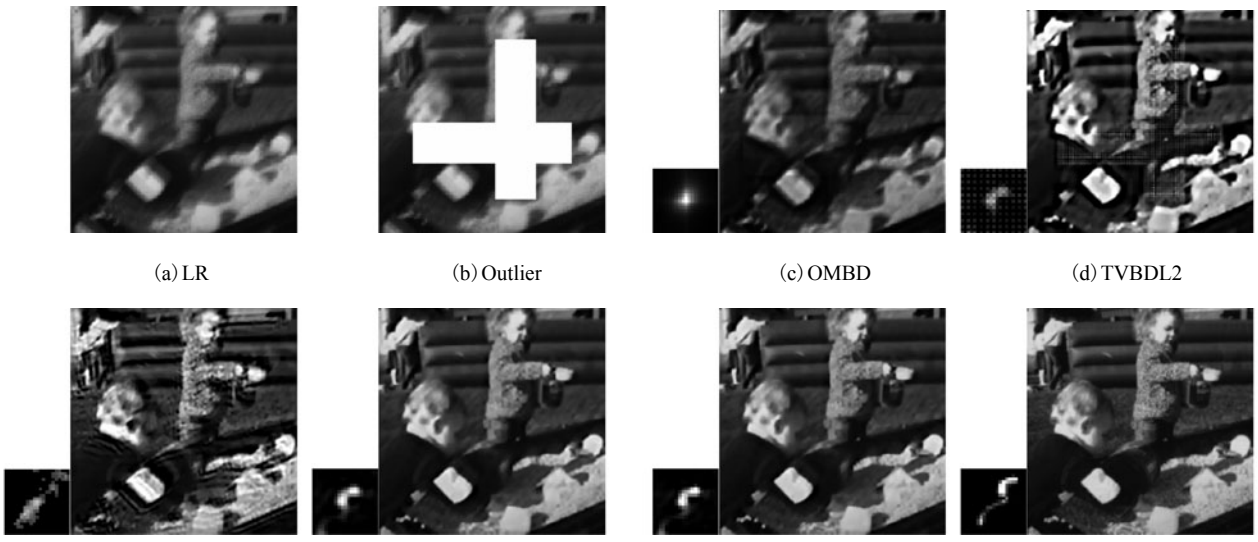

(a) LR (b) Outlier (c) OMBD (d) TVBDL2

(e) BKE (f) TVBD (g) MBSRI based on MSAA (h) Ground truth

Fig. 7 Results with the blur size of 21 × 21 and the outlier influence

Tab. 4 Comparison data of the outlier experiment with the 13 × 13 blur kernel

Algorithm	SSIM	PSNR	SSD	MSE
TVBDL2	0.851	25.371	134.207	2.903×10^{-3}
BKE	0.921	29.346	53.735	1.163×10^{-3}
TVBD	0.971	34.278	17.263	3.735×10^{-4}
MBSRI based on MSAA	0.975	35.013	14.574	3.153×10^{-4}

Tab. 5 Comparison data of the outlier experiment with the 21 × 21 blur kernel

Algorithm	SSIM	PSNR	SSD	MSE
TVBDL2	0.672	20.060	455.893	9.863×10^{-3}
BKE	0.638	20.950	371.456	8.036×10^{-3}
TVBD	0.926	31.093	35.938	7.775×10^{-4}
MBSRI based on MSAA	0.935	31.886	29.946	6.478×10^{-4}

4 Conclusions

(1) MBSRI algorithm based on TVBD can solve the MBSRI problem when the unknown blur kernel contains more details. The experimental results demonstrate its efficiency and superiority.

(2) MBSRI algorithm based on MSAA can enhance the image spatial resolution when the LR images contain some outliers. Compared with the state-of-the-art algorithms, the proposed algorithm shows the best performance. The experimental results underline and confirm its high quality, accuracy and simplicity.

References

[1] Wirawan P D, Maitre H. Multi-channel high resolution blind image restoration[C]. In: *Proceedings of IEEE International Conference on Acoustics, Speech, and Signal Processing*. Phoenix, USA, 1999.

[2] Freeman W T, Pasztor E C. Learning to estimate scenes from images[C]. In: *Advances in Neural Information Processing Systems*. 1998.

[3] Sroubek F, Cristóbal G, Flusser J. Simultaneous super-resolution and blind deconvolution[J]. *Journal of Physics: Conference Series*, 2008, 124(1): 012048.

[4] Mudenagudi U, Singla R, Kalra P *et al*. Super resolution using graph-cut[C]. In: *Proceedings of 7th Asian Conference on Computer Vision*. Hyderabad, India, 2006.

[5] Peleg T, Elad M. A statistical prediction model based on sparse representations for single image super-resolution[J]. *IEEE Transactions on Image Processing*, 2014, 23(6): 2569-2582.

[6] Fattal R. Image upsampling via imposed edge statistics[J]. In: *ACM Transactions on Graphics (TOG)*, 2007, 26(3): 95.

[7] Efrat N, Glasner D, Apartsin A *et al*. Accurate blur models vs. image priors in single image super-resolution[C]. In: *Proceedings of IEEE International Conference on Computer Vision (ICCV)*. Sydney, Australia, 2013.

[8] Wang Q, Tang X, Shum H. Patch based blind image super resolution[C]. In: *Proceedings of* 10*th IEEE International Conference on Computer Vision (ICCV)*. Beijing, China, 2005.

[9] Harmeling S, Sra S, Hirsch M *et al*. Multiframe blind deconvolution, super-resolution, and saturation correction via incremental EM[C]. In: *Proceedings of 17th IEEE International Conference on Image Processing (ICIP)*. Hong Kong, China, 2010.

[10] Levin A, Weiss Y, Durand F *et al*. Understanding blind deconvolution algorithms[J]. *IEEE Transactions on Pattern Analysis and Machine Intelligence*, 2011, 33(12): 2354-2367.

[11] Perrone D, Favaro P. Total variation blind deconvolution: The devil is in the details[C]. In: *Proceedings of IEEE Conference on Computer Vision and Pattern Recognition (CVPR)*. Columbus, USA, 2014.

[12] Michaeli T, Irani M. Nonparametric blind super-resolution [C]. In: *Proceedings of IEEE International Conference on Computer Vision (ICCV)*. Sydney, Australia, 2013.

[13] Farsiu S, Robinson M D, Elad M *et al*. Fast and robust multiframe super resolution [J]. *IEEE Transactions on Image Processing*, 2004, 13(10): 1327-1344.

[14] Sroubek F, Milanfar P. Robust multichannel blind deconvolution via fast alternating minimization[J]. *IEEE Transactions on Image Processing*, 2012, 21(4): 1687-1700.

[15] Shan Q, Jia J, Agarwala A. High-quality motion deblurring from a single image[J]. *ACM Transactions on Graphics (TOG)*, 2008, 27(3): 73.

[16] Xu L, Jia J. Two-phase kernel estimation for robust motion deblurring[C]. In: *Proceedings of Computer Vision-ECCV* 2010. Heraklion, Greece, 2010.

[17] Windows Image Acquisition[EB/OL]. https://en. wikipedia.org/wiki/Windows_Image_ Acquisition, 2016-07-05.

[18] Lertrattanapanich S, Bose N K. High resolution image formation from low resolution frames using Delaunay triangulation[J]. *IEEE Transactions on Image Processing*, 2002, 11(12): 1427-1441.

[19] Rudin L I, Osher S, Fatemi E. Nonlinear total variation based noise removal algorithms[J]. *Physica D: Nonlinear Phenomena*, 1992, 60(1-4): 259-268.

[20] Rameshan R M, Chaudhuri S, Velmurugan R. Joint MAP estimation for blind deconvolution: When does it work? [C]. In: *Proceedings of the 8th Indian Conference on Computer Vision, Graphics and Image Processing*. Mumbai, India, 2012.

[21] Thompson A M, Brown J C, Kay J W *et al*. A study of methods of choosing the smoothing parameter in image restoration by regularization[J]. *IEEE Transactions on Pattern Analysis & Machine Intelligence*, 1991, 13(4): 326-339.

[22] Eldar Y C. Generalized SURE for exponential families: Applications to regularization[J]. *IEEE Transactions on Signal Processing*, 2009, 57(2): 471-481.

[23] Ramani S, Liu Z, Rosen J *et al*. Regularization parameter selection for nonlinear iterative image restoration and MRI reconstruction using GCV and SURE-based methods[J]. *IEEE Transactions on Image Processing*, 2012, 21(8): 3659-3672.

[24] Hirsch M, Harmeling S, Sra S *et al*. Online multiframe blind deconvolution with super-resolution and saturation correction[J]. *Astronomy & Astrophysics*, 2011, 531: A9.

[25] Harmeling S, Hirsch M, Sra S *et al*. Online blind deconvolution for astronomical imaging[C]. In: *Proceedings of IEEE International Conference on Computational Photography (ICCP)*. San Francisco, USA, 2009.

[26] Goldstein A, Fattal R. Blur-kernel estimation from spectral irregularities[C]. In: *Proceedings of Computer Vision-ECCV* 2012. Florence, Italy, 2012.

(Editor: Wu Liyou)